An Analytical and Numerical Investigation of Rayleigh Wave Scattering by a Surface Defect in Orthotropic Media

Hoang Ngoc Quy
Institute of Mechanics, Vietnam Academy of Science and Technology, Vietnam | Faculty of Civil Engineering, VNU University of Engineering and Technology, Vietnam
hnquy@imech.vast.vn

Truong Giang Nguyen
Institute of Mechanics, Vietnam Academy of Science and Technology, Vietnam | Faculty of Engineering Mechanics and Automation, VNU University of Engineering and Technology, Vietnam
ntgiang@imech.vast.vn (corresponding author)

Received: 28 October 2025 | Revised: 22 November 2025 | Accepted: 9 December 2025

 DOI: https://doi.org/10.48084/etasr.15836

ABSTRACT

This study presents a reciprocity-based analytical model for Rayleigh wave scattering by localized surface defects in orthotropic elastic half-spaces. Closed-form expressions for forward and backward scattering amplitudes are derived directly from the elastodynamic reciprocity theorem, linking the scattered field to defect geometry and excitation frequency without numerical discretization. Finite-element comparisons confirmed the accuracy and robustness of the proposed approach across a wide parameter range. The results show that scattering is primarily governed by the defect's width-to-depth ratio: broader and shallower cavities yield smoother and more stable responses, whereas deeper defects cause slightly stronger discrepancies. The proposed compact formulation offers a clear physical interpretation of wave–defect interaction and practical guidance for Nondestructive Evaluation (NDE) and Structural Health Monitoring (SHM) in anisotropic and orthotropic media.

Keywords-Rayleigh wave; orthotropic; reciprocity theorem; wave scattering; nondestructive evaluation; structural health monitoring

I. INTRODUCTION

Rayleigh waves exhibit high sensitivity to surface and near-surface defects, enabling their effective use in NDE and SHM [1, 2]. Advanced signal-processing methods, such as the chirplet transform, have further improved defect detection and characterization [3]. During propagation, these waves interact with cracks, voids, and corrosion pits, generating scattered and reflected fields that reveal the defect geometry [4-6].

Analytical scattering models provide valuable physical insights and form the theoretical foundation for many characterization methods. Classical isotropic formulations, pioneered by Gilbert and Knopoff through potential and boundary perturbation methods [7], offer essential intuition but are limited to simplified geometries and assumptions. Numerical approaches, such as the Finite Element Method (FEM) and Boundary Element Method (BEM), allow the analysis of arbitrary defect shapes and complex boundaries [8-10]. However, they often lack the compactness and interpretability of analytical solutions.

To overcome these limitations, reciprocity-based formulations have been introduced [11, 12] and later extended to surface and interface waves [13, 14], providing closed-form expressions that combine the rigorous elastodynamic theory with computational efficiency and physical transparency. Building on earlier studies of wave propagation in layered anisotropic composites [15], recent research has increasingly focused on anisotropic and orthotropic media, where direction-dependent stiffness and polarization lead to variations in the Rayleigh wave velocity, attenuation, and scattering amplitude with the propagation direction [16, 17]. While FEM and BEM simulations can handle these complexities [18, 19], analytical solutions remain limited due to the inherent mathematical difficulty of anisotropy.

In orthotropic solids, the interplay between material anisotropy and defect geometry (depth, width, and aspect ratio) critically influences Rayleigh wave scattering. Developing an analytical framework that explicitly links these parameters to the scattered field is therefore vital for advancing wave-based defect characterization in anisotropic materials. Motivated by this gap, the present work develops a reciprocity-based

analytical framework for Rayleigh-wave scattering by a localized surface defect in an orthotropic half-space. Closed-form forward and backward scattering amplitudes are derived and validated against finite element simulations. The influence of defect geometry and excitation frequency on the scattered field is then analyzed, providing practical insights for NDE and SHM applications in orthotropic materials.

II. SCATTERING OF RAYLEIGH WAVES BY A SURFACE DEFECT IN AN ORTHOTROPIC HALF-SPACE

Rayleigh-wave scattering by a localized surface defect in an orthotropic half-space is studied using the elastodynamic reciprocity theorem, with basic formulations taken from [17]. A time-harmonic Rayleigh wave of amplitude A_{in}, propagating in the positive x_1-direction, impinges on the defect (Figure 1(a)). The total displacement field expressed as $\boldsymbol{u} = \boldsymbol{u}_{in} + \boldsymbol{u}_{sc}$, includes both the incident and scattered components (Figures 1(b–c)). The scattered field $\boldsymbol{u}_{\text{sc}}$ is generated by equivalent distributed normal and tangential tractions acting along the boundary of the defect. Subsequently, this study focuses on the configuration in Figure 1(c), considering forward and backscattering of Rayleigh waves and the corresponding amplitude ratios with respect to the incident amplitude A_{in}.

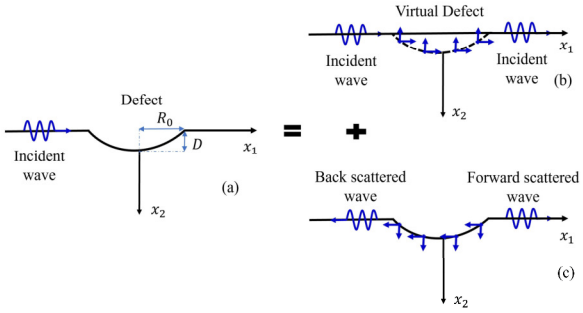

Fig. 1. Linear superposition principle.

For definiteness, the defect is modeled as a symmetric circular cavity of maximum depth D and total width $2R_0$ along x_1(Figure 1(a)). Its boundary is described by the graphs $x_2 = h(x_1)$, in which:

$$h(x_1) = \sqrt{\left(\frac{R_0^2+D^2}{2D}\right)^2 - x_1^2} - \frac{R_0^2-D^2}{2D} \quad (1)$$

Differentiating (1) gives $h'(x_1)$. The unit normal is $\boldsymbol{n} = \left(n_{x_1}, n_{x_2}\right)$ and the boundary line element is $\mathrm{d}S = \sqrt{1+[h'(x_1)]^2}\,\mathrm{d}x_1$. The associated horizontal and vertical loads in Figure 1(c) are evaluated at (x_1^0, x_2^0) as:

$$f_{x_1}(x_1^0, x_2^0) = \sigma_{11}(x_1^0, x_2^0)h'(x_1^0)dx_1^0 - \sigma_{12}(x_1^0, x_2^0)dx_1^0 \quad (2)$$

$$f_{x_2}(x_1^0, x_2^0) = \sigma_{12}(x_1^0, x_2^0)h'(x_1^0)dx_1^0 - \sigma_{22}(x_1^0, x_2^0)dx_1^0 \quad (3)$$

Using the stress expressions of the incident Rayleigh wave reported in [17], yields the distributed load components acting along the cavity boundary:

$$f_{x_1}(x_1^0, x_2^0) = A_{in}[ikc_{66}T_{11}(x_2^0)h'(x_1^0) + kc_{66}T_{12}(x_2^0)]e^{ik(x_1-ct)}dx_1^0 \quad (4)$$

$$f_{x_2}(x_1^0, x_2^0) = A_{in}[-kc_{66}T_{12}(x_2^0)h'(x_1^0) - ikc_{66}T_{22}(x_2^0)]e^{ik(x_1-ct)}dx_1^0 \quad (5)$$

where T_{11}, T_{12}, and T_{22} are the dimensionless stress-distribution functions of the incident Rayleigh wave, whose explicit forms are provided in [17]. These distributed loads give rise to scattered Rayleigh wave fields radiating along both surface directions.

Using the expression for the wave amplitude generated by a force given in [17], the forward and backward scattered Rayleigh-wave amplitudes are obtained by integrating the scattered contributions along the cavity boundary:

$$\left|\frac{A_{sc}^{+}}{A_{in}}\right| = \left|\frac{\int_{-R_0}^{R_0} F^{+}(x_1^0, x_2^0)dx_1^0}{2C_{66}I}\right| \quad (6)$$

$$\left|\frac{A_{sc}^{-}}{A_{in}}\right| = \left|\frac{\int_{-R_0}^{R_0} F^{-}(x_1^0, x_2^0)e^{2ikx_1^0}dx_1^0}{2C_{66}I}\right| \quad (7)$$

where:

$$F^{+}(x_1^0, x_2^0) = [-kC_{66}T_{12}(x_2^0)h'(x_1^0) - ikC_{66}T_{22}(x_2^0)]U_2(x_2^0) + [-kC_{66}T_{11}(x_2^0)h'(x_1^0) + ikC_{66}T_{12}(x_2^0)]U_1(x_2^0) \quad (8)$$

$$F^{-}(x_1^0, x_2^0) = [-kC_{66}T_{12}(x_2^0)h'(x_1^0) - ikC_{66}T_{22}(x_2^0)]U_2(x_2^0) + [kC_{66}T_{11}(x_2^0)h'(x_1^0) - ikC_{66}T_{12}(x_2^0)]U_1(x_2^0) \quad (9)$$

This formulation yields closed-form tractions for an incident Rayleigh wave on a traction-free cavity in an orthotropic medium. Inserting these loads into the reciprocity framework gives analytical amplitude ratios for forward and backward scattered waves, as given in (6) and (7), reducing the reliance on purely numerical methods and improving clarity and efficiency. The expressions depend explicitly on defect geometry (R_0, D) and the medium's elastic constants, so anisotropy enters directly. This analytical tool supports the practical prediction of scattered waves for NDE and SHM.

III. RESULTS AND DISCUSSION

The analytical formulation was validated and the scattering behavior was examined under various conditions. First, closed-form predictions for an orthotropic half-space without defects are compared with full-wave FEM simulations for two representative loading scenarios: (1) a time-harmonic distributed normal traction on the free surface and (2) a time-harmonic distributed load embedded at a certain depth. Next, the formulation is applied to a surface cavity defect, reporting the bidirectional scattering amplitude ratios $\frac{A_{\text{sc}}^{+}}{A_{\text{in}}}$ and $\frac{A_{\text{sc}}^{-}}{A_{\text{in}}}$ (forward and backward, respectively) and investigating how the scattered response is governed by excitation frequency and defect geometry (characterized by cavity width $2R_0$ and depth D). All calculations used the material properties of the Beryl rock, with the orthotropic elastic constants taken from [20] and listed in Table I.

TABLE I. MATERIAL PROPERTIES OF THE HALF-SPACE

Material	$\rho\left(\frac{\mathbf{kg}}{\mathbf{m^3}}\right)$	C_{11}(Gpa)	C_{12}(Gpa)	C_{22}(Gpa)	C_{66}(Gpa)
Beryl rock	2500	36.2	10.1	41.3	13.3

A. *Model Verification*

This study first validates the analytical expressions for the forward and backward Rayleigh wave amplitude ratios $\frac{A_{sc}^{\pm}}{A_{in}}$ by comparing them with FEM simulations (COMSOL Multiphysics) under the two loading configurations described above. The simulations employ a single-frequency (monochromatic) excitation. For the chosen frequency (angular frequency ω), the Rayleigh secular equation for the orthotropic half-space is solved to obtain the Rayleigh wave phase velocity c. Both the analytical and numerical models use identical material and geometric parameters to ensure a fair comparison.

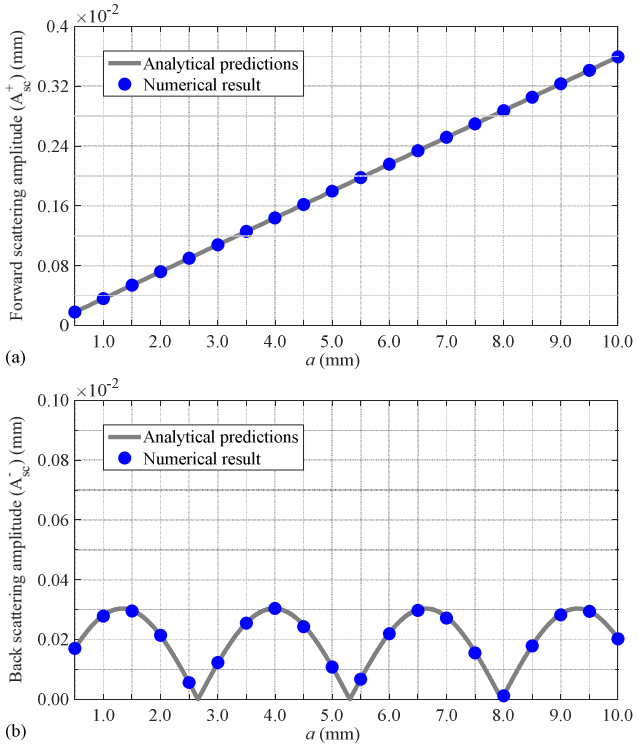

Fig. 2. Surface line load case: validation of (a) forward and (b) backward scattering amplitudes.

1) *Distributed Surface Load*

In this scenario, a time-harmonic normal traction with reference amplitude $P = C_{66}$, is applied over a finite surface strip defined by $-a \le x_1 \le a$ at $x_2 = 0$ (total width $2a$). The analytical scattering predictions are obtained by integrating the point-load solutions in (6) and (7) over the strip $[-a, a]$. The half-width a is varied from zero up to several Rayleigh wavelengths and the resulting forward and backward amplitude ratios A_{sc}^{+} and A_{sc}^{-} are benchmarked against finite-element results. As shown in Figure 2(a) (forward) and 2(b) (backward), the agreement between the theory and simulation is excellent. The forward-scattered amplitude increases smoothly as the strip width expands, consistent with the coherent addition of contributions across a broader aperture. In contrast, the backward-scattered amplitude oscillates as a increases because of the oscillatory exponential term in (7). This factor oscillates, as does the resulting scattered amplitude, which is captured well by the analytical model and shows excellent agreement with the numerical results.

2) *Distributed Subsurface Load*

In this case, the strip half-width is fixed at $a = 2$ mm while the load is embedded at depths D ranging from 0.5 to 5 mm. The forward amplitude A_{sc}^{+} (Figure 3(a)) decreases steadily as the source depth increases, and the analytical curve closely follows the numerical data across the entire tested range. The backward amplitude A_{sc}^{-} (Figure 3(b)) exhibits a similar downward trend with increasing depth, again with near-perfect agreement between the analytical solution and simulation. Across both validation cases, the surface strip load and the subsurface embedded load, the analytical predictions closely match the FEM results over the full range of strip widths and depths considered. The model correctly reproduces the smooth increase in the forward-scattered amplitude with a larger surface loading area, interference-induced oscillations in the backward-scattered amplitude, and decay of both amplitudes with increasing source depth. These comparisons provide a strong validation of the reciprocity-based analytical framework for an orthotropic half-space. This successful verification builds confidence in applying the model to the more complex case of a surface cavity, which is addressed next.

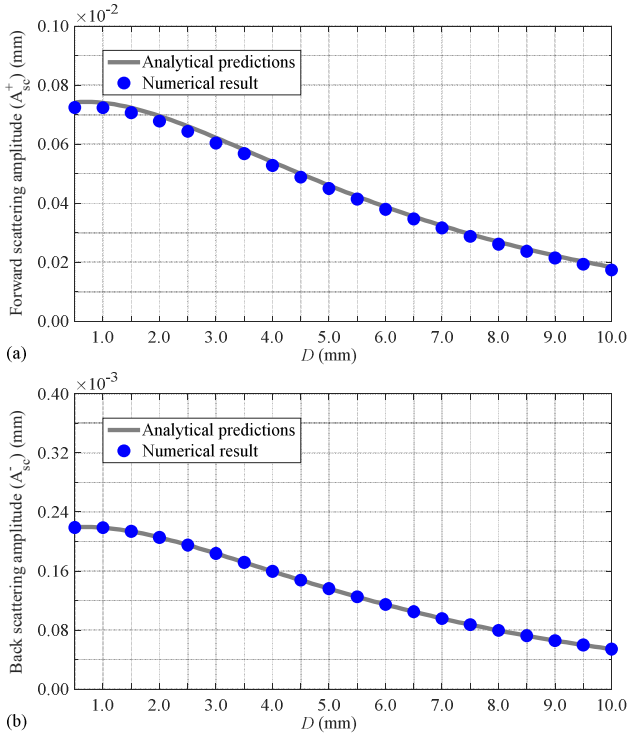

Fig. 3. Subsurface line load case: validation of: (a) forward and (b) backward scattering amplitudes.

B. Cavity Scattering Results

Following the above validation, this work now turns to the problem of Rayleigh wave scattering by a localized surface cavity. This configuration represents a geometric defect in the half-space (as opposed to an applied load), providing a more stringent test of the analytical model developed in Section II. The cavity is idealized as a cylindrical void characterized by a half-width R_0 and a maximum depth D below the free surface. Using the same reciprocity-based framework, closed-form expressions were derived for the forward and backward scattered wave amplitude ratios A_{sc}^{+} and $A_{sc,}^{-}$ normalized by the incident Rayleigh wave amplitude. These analytical predictions were then benchmarked against finite element simulations performed under identical material properties, cavity geometry, and excitation conditions. By comparing the results, the accuracy and applicability of the proposed formulas are assessed as functions of the cavity geometry and the excitation frequency.

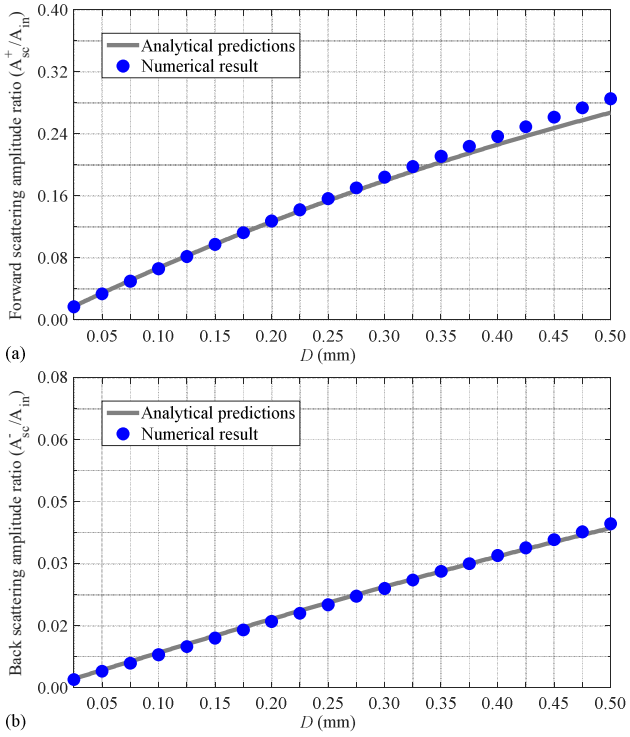

Fig. 4. Normalized scattering amplitude ratios versus cavity depth D at $f = 0.2$ MHz, $R_0 = 5.0$ mm: (a) forward scattering and (b) back scattering.

The present study first considered a cylindrical cavity with fixed half-width $R_0 = 5.0$ mm and excitation frequency $f = 0.2$ MHz, while the cavity depth D varied from 0.025 to 0.5 mm. Figure 4 illustrates the normalized forward and backward scattering amplitude ratios $|\frac{A_{sc}^{+}}{A_{in}}|$ and $|\frac{A_{sc}^{-}}{A_{in}}|$ as functions of D, with analytical predictions plotted as continuous curves and finite-element results shown as discrete markers. In the forward direction (Figure 4(a)), the FEM data closely follow the analytical curve for all considered depths, with only slight deviations appearing at the largest cavity depths. The backward-scattered results (Figure 4(b)) exhibit a similar agreement: the analytical and numerical curves coincide over most of the depth range, and only minor differences emerge as D increases. These discrepancies at greater depths are small and remain within acceptable bounds. Overall, the depth-sweep results demonstrate that the proposed analytical formulation provides accurate and stable predictions for shallow to moderately deep cavities, and it still performs satisfactorily even as the cavity becomes deeper within the tested range.

Next, the influence of cavity width on scattering is investigated, while keeping the depth and frequency fixed at $D = 0.2$ mm and $f = 0.2$ MHz, respectively. For forward scattering (Figure 5(a)), the amplitude ratio increases nearly linearly with R_0. The analytical predictions (curve) agree well with the FEM results (markers) across the range of widths, with only some noticeable differences at the smallest widths and a few minor deviations at the largest widths. In the backward direction (Figure 5(b)), both the analytical and numerical results showed an oscillatory dependence on the cavity width. The first few oscillations (at small widths) display some discrepancy in amplitude between the model and simulation, but the agreement improves as the cavity width increases. Overall, the analytical model accurately captures the width-dependent trends in both forward and backward scattering, with higher precision observed for wider (more laterally extended) cavities. These results also suggest that the width-to-depth aspect ratio of the cavity plays a role in the model's accuracy: as this aspect ratio grows, the analytical predictions tend to become more stable and reliable (within the model's assumptions), although small localized differences can still occur at certain widths.

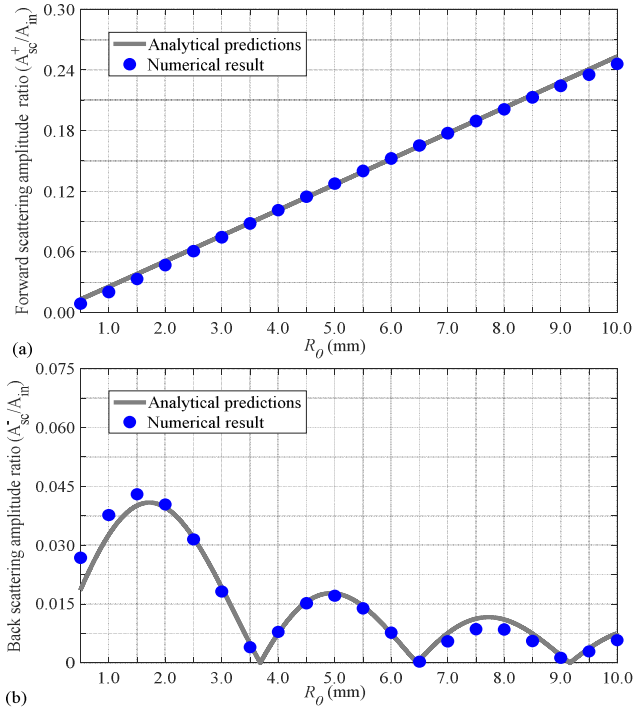

Fig. 5. Normalized scattering amplitude ratios versus cavity width R_0 at $f = 0.2$ MHz, $D = 0.2$ mm: (a) forward scattering and (b) back scattering.

To evaluate the combined effects of geometry and frequency, this study conducted a parametric study over a range of cavity aspect ratios and excitation frequencies. Specifically, three representative cavity configurations were considered, with width-to-depth aspect ratios of approximately 6, 8, and 10. These cases span a practical range from relatively deep/narrow cavities (lower aspect ratio) to shallow/broad cavities (higher aspect ratio), allowing the assessment of the model under different geometric extremes. For each configuration, the normalized forward and backward scattering ratios were calculated over a band of excitation frequencies (covering a range from low to high frequencies relevant to the material and cavity size), and the analytical predictions were compared to FEM results at each frequency. Figures 6–8 summarize these comparisons, illustrating how the frequency response of the scattered amplitudes is affected by the cavity aspect ratio.

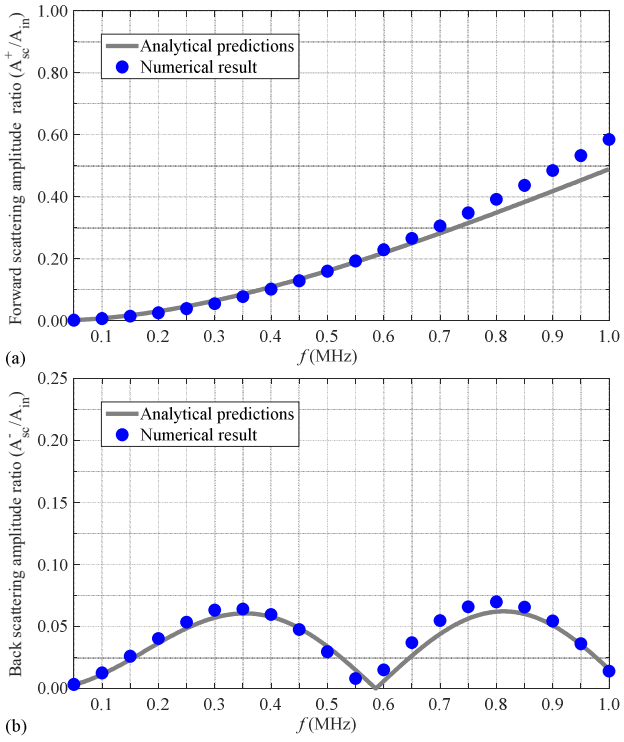

Fig. 6. Normalized forward and backward scattering amplitude ratios for the cavity case with $R_0/D = 6$: (a) forward scattering and (b) back scattering.

A clear trend emerges from these frequency-domain results. As the cavity aspect ratio increases from 6 up to 10, the overall scattering response becomes more stable and predictable, with a smoother frequency dependence in both the forward and backward directions. At $R_0/D = 6$ (Figure (6)), noticeable discrepancies are observed between the analytical and numerical curves, particularly toward the higher end of the frequency range. When the aspect ratio is increased to $R_0/D = 8$ (Figure 7), the agreement improves across most of the spectrum, and the oscillatory behavior of the backward-scattered amplitude becomes more consistent between the two methods. At the highest aspect ratio, $R_0/D = 10$ (Figure 8), the backward-scattering predictions are nearly exact across the entire frequency range, whereas the forward scattering still shows a slight deviation at the highest frequencies. However, this deviation is much smaller than those seen in the lower aspect ratio cases. These results indicate that larger cavity aspect ratios (i.e. laterally extensive but shallow cavities) generally provide the most favorable conditions for the analytical model, particularly for the backward-scattered wave. In contrast, cavities with smaller aspect ratios (deeper or narrower defects) tend to produce slightly greater discrepancies between the analytical and FEM results. In other words, the analytical model is most accurate for shallow defects (large R_0/D). As the aspect ratio decreases, i.e., the cavity becomes deeper or narrower, the discrepancies with the FEM results increase modestly. Agreement also remains strong when the defect width is small compared with the wavelength, since the model assumptions are then well satisfied.

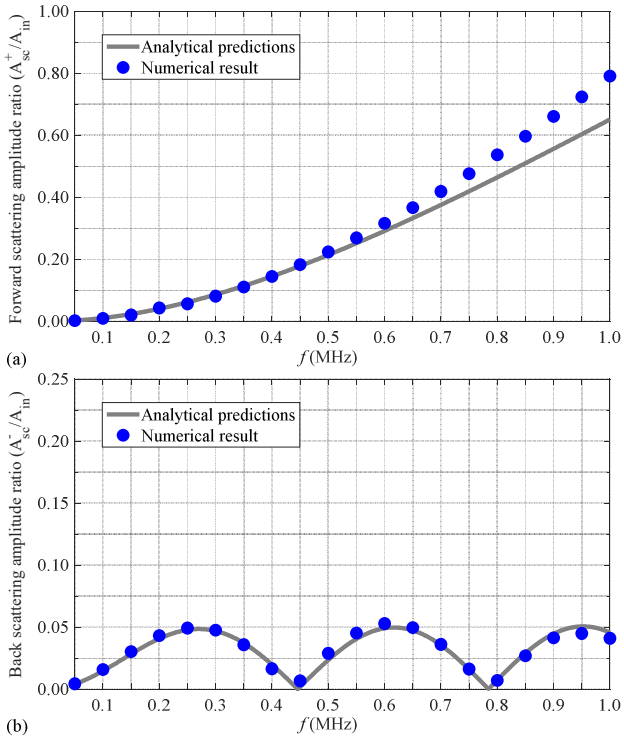

Fig. 7. Normalized forward and backward scattering amplitude ratios for the cavity case with $R_0/D = 8$: (a) forward scattering and (b) back scattering.

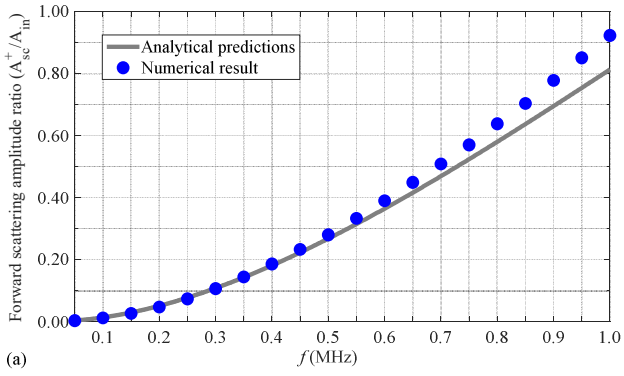

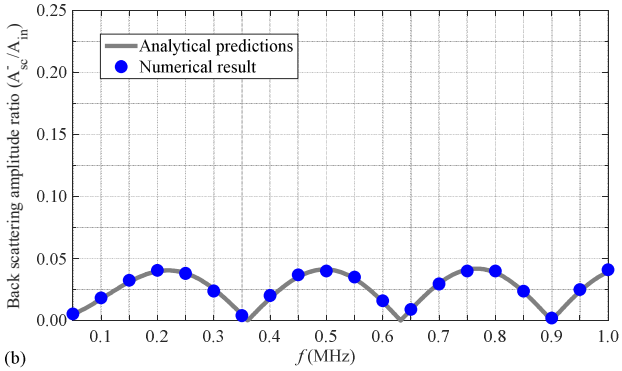

Fig. 8. Normalized forward and backward scattering amplitude ratios for the cavity case with $R_0/D = 10$: (a) forward scattering and (b) back scattering.

In summary, the proposed reciprocity-based analytical model provides reliable predictions of Rayleigh wave scattering in all considered cases, showing close agreement with the numerical results for cavity defects. Over the tested geometric range, accuracy improves as the cavity width-to-depth ratio increases, with the best performance observed for wide, shallow defects that yield smooth scattering responses. The model also performs most consistently when the width-to-wavelength ratio ($\frac{R_0}{\lambda}$) is small, in line with the assumptions underlying the analytical formulation. For deeper cavities, discrepancies grow as near-field disturbances become stronger, and aspect ratios far beyond the investigated range are expected to produce larger deviations from FEM. Overall, the closed-form approach captures the key scattering behavior in orthotropic media and highlights the dominant role of defect geometry, particularly the aspect ratio.

IV. CONCLUSIONS

A reciprocity-based analytical framework is presented for Rayleigh wave scattering by a surface cavity in an orthotropic elastic half-space. The resulting closed-form expressions relate the scattered field directly to the defect geometry and excitation frequency, enabling the efficient evaluation of forward and backward scattering without numerical discretization. The analytical approach showed excellent agreement over a wide parameter range with the Finite Element Method (FEM) simulations, confirming the accuracy and robustness of the model. The results also demonstrate that scattering is governed primarily by cavity geometry, especially the width-to-depth ratio, and by defect size relative to the wavelength, captured by the width-to-wavelength ratio. These factors determine the smoothness and stability of the scattered amplitudes. This constitutes the main practical contribution and novelty of the study and provides a solid basis for future extensions to more complex defect shapes, multilayer media, and coupled thermoelastic effects.

The analytical solutions also enable the rapid evaluation of wavefields at any point, with a far lower computational cost than FEM, which is particularly advantageous for inverse Nondestructive Evaluation (NDE) and Structural Health Monitoring NDE/SHM, and material characterization problems requiring many forward simulations. Moreover, the closed forms make parameter effects explicit, offering clearer physical insight into how geometry and anisotropy influence scattering.

ACKNOWLEDGMENT

This research was funded by the Vietnam Academy of Science and Technology under grant number CSCL03.03/24-25.

REFERENCES

[1] R. Al Wardany, J. Rhazi, G. Ballivy, J. L. Gallias, and K. Saleh, "Use of Rayleigh wave methods to detect near surface concrete damage," presented at the *16th World Conference on NDT*, Montreal, Canada, 2004.

[2] J. L. Rose, *Ultrasonic Guided Waves in Solid Media*. New York: Cambridge University Press, 2014.

[3] M. S. Mohammed and K. Ki-Seong, "Chirplet Transform in Ultrasonic Non-Destructive Testing and Structural Health Monitoring: A Review," *Engineering, Technology & Applied Science Research*, vol. 9, no. 1, pp. 3778–3781, Feb. 2019, https://doi.org/10.48084/etasr.2470.

[4] R. Ávila-Carrera, A. Rodríguez-Castellanos, F. J. Sánchez-Sesma, and C. Ortiz-Alemán, "Rayleigh-wave scattering by shallow cracks using the indirect boundary element method," *Journal of Geophysics and Engineering*, vol. 6, no. 3, May 2009, Art. no. 221, https://doi.org/10.1088/1742-2132/6/3/002.

[5] A. Rodríguez-Castellanos, R. Ávila-Carrera, and F. J. Sánchez-Sesma, "Scattering of Rayleigh-waves by surface-breaking cracks: an integral formulation," *Geofísica Internacional*, vol. 46, no. 4, pp. 241–248, 2007, https://doi.org/10.22201/igeof.00167169p.2007.46.4.48.

[6] P. H. Dang, L. D. Tho, L. Q. Hung, and D. D. Kien, "Investigation of Rayleigh wave interaction with surface defects," *Journal of Science and Technology in Civil Engineering - NUCE*, vol. 13, no. 3, pp. 95–103, Aug. 2019, https://doi.org/10.31814/stce.nuce2019-13(3)-09.

[7] F. Gilbert and L. Knopoff, "Seismic scattering from topographic irregularities," *Journal of Geophysical Research*, vol. 65, no. 10, pp. 3437–3444, 1960, https://doi.org/10.1029/JZ065i010p03437.

[8] G. Hévin, O. Abraham, H. A. Pedersen, and M. Campillo, "Characterization of surface cracks with Rayleigh waves: a numerical model," *NDT & E International*, vol. 31, no. 4, pp. 289–297, Aug. 1998, https://doi.org/10.1016/S0963-8695(98)80013-3.

[9] W. Hassan and W. Veronesi, "Finite element analysis of Rayleigh wave interaction with finite-size, surface-breaking cracks," *Ultrasonics*, vol. 41, no. 1, pp. 41–52, Jan. 2003, https://doi.org/10.1016/S0041-624X(02)00393-1.

[10] S. Zhang, Y. Liu, L. Wang, and F. Wang, "Scattering of Rayleigh wave by inclined surface open cracks: Numerical simulations based on reciprocity theorem and verification using finite element method," *Applied Mathematical Modelling*, vol. 145, Sept. 2025, Art. no. 116147, https://doi.org/10.1016/j.apm.2025.116147.

[11] J. D. Achenbach, *Wave Propagation in Elastic Solids: North-Holland Series in Applied Mathematics and Mechanics*. North Holland/Elsevier, 2013.

[12] J. D. Achenbach and Y. Xu, "Use of elastodynamic reciprocity to analyze point-load generated axisymmetric waves in a plate," *Wave Motion*, vol. 30, no. 1, pp. 57–67, July 1999, https://doi.org/10.1016/S0165-2125(98)00050-X.

[13] H. Phan, Y. Cho, and J. D. Achenbach, "Application of the reciprocity theorem to scattering of surface waves by a cavity," *International Journal of Solids and Structures*, vol. 50, no. 24, pp. 4080–4088, Nov. 2013, https://doi.org/10.1016/j.ijsolstr.2013.08.020.

[14] H. Phan, T. Q. Bui, H. T.-L. Nguyen, and C. V. Pham, "Computation of interface wave motions by reciprocity considerations," *Wave Motion*,

vol. 79, pp. 10–22, June 2018, https://doi.org/10.1016/j.wavemoti.2018.02.008.

[15] S. I. Rokhlin and L. Wang, "Ultrasonic waves in layered anisotropic media: characterization of multidirectional composites," *International Journal of Solids and Structures*, vol. 39, no. 16, pp. 4133–4149, Aug. 2002, https://doi.org/10.1016/S0020-7683(02)00363-3.

[16] P. C. Vinh and R. W. Ogden, "On the Rayleigh Wave Speed in Orthotropic Elastic Solids," *Meccanica*, vol. 40, no. 2, pp. 147–161, Apr. 2005, https://doi.org/10.1007/s11012-005-1603-6.

[17] D. K. Dao, V. Ngo, H. Phan, C. V. Pham, J. Lee, and T. Q. Bui, "Rayleigh wave motions in an orthotropic half-space under time-harmonic loadings: A theoretical study," *Applied Mathematical Modelling*, vol. 87, pp. 171–179, Nov. 2020, https://doi.org/10.1016/j.apm.2020.06.006.

[18] C. Yang, B. Wang, Z. Qian, and S. Hirose, "Modified BEM for scattering analysis by a flaw at interface in an anisotropic multi-layered plate," *Engineering Analysis with Boundary Elements*, vol. 152, pp. 704–727, July 2023, https://doi.org/10.1016/j.enganabound.2023.04.028.

[19] S. Li, M. Huang, Y. Song, B. Lan, and X. Li, "Theoretical and numerical modeling of Rayleigh wave scattering by an elastic inclusion," *The Journal of the Acoustical Society of America*, vol. 153, no. 4, Apr. 2023, Art. no. 2336, https://doi.org/10.1121/10.0017837.

[20] A. Khojasteh, M. Rahimian, M. Eskandari, and R. Y. S. Pak, "Asymmetric wave propagation in a transversely isotropic half-space in displacement potentials," *International Journal of Engineering Science*, vol. 46, no. 7, pp. 690–710, July 2008, https://doi.org/10.1016/j.ijengsci.2008.01.007.